Supporting Information for

Controlling the Orientation, Edge Geometry and Thickness of Chemical Vapor Deposition Graphene

Adrian T. Murdock[1], Antal A. Koos[1], T. Ben Britton[1], Lothar Houben[2], Tim Batten[3], Tong Zhang[3], Angus J. Wilkinson[1], Rafal Dunin-Borkowski[2], Christina E. Lekka[4], and Nicole Grobert[1,]*

[1]Department of Materials, University of Oxford, Oxford OX1 3PH, UK

[2]Ernst Ruska Centre for Microscopy and Spectroscopy with Electrons, Forschungszentrum Juelich GmbH, 52425 Juelich, Germany

[3]Renishaw plc, Old Town, Wotton-under-Edge, Gloucestershire, GL12 7DW, UK

[4]Department of Materials Science and Engineering, University of Ioannina, 45110 Ioannina, Greece

*email: nicole.grobert@materials.ox.ac.uk

Additional OM, SEM and EBSD maps illustrating variation of shape and orientation of LPCVD graphene domains on different Cu crystallographic orientations

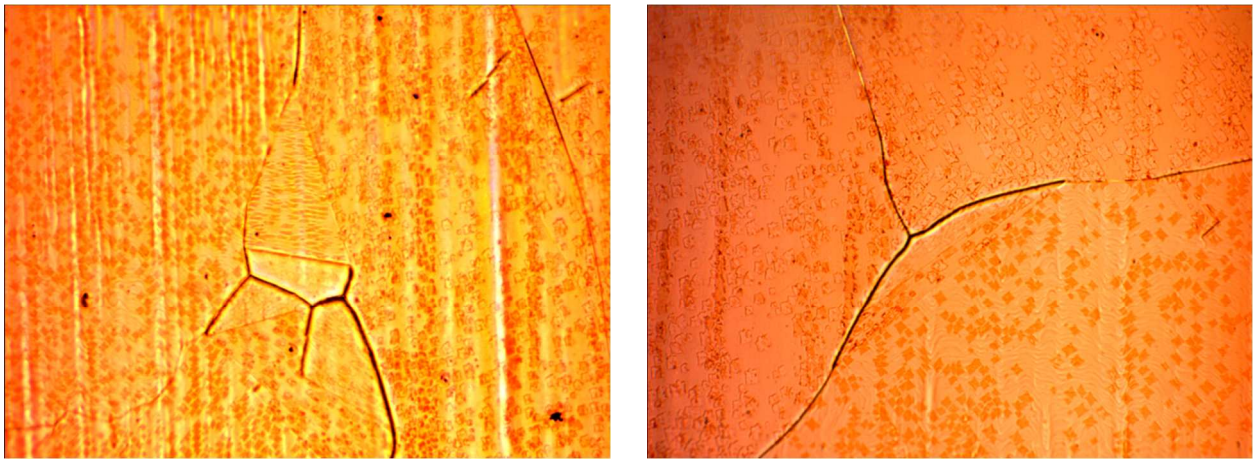

Figure S1| Optical micrographs of the Cu surface after LPCVD graphene formation showing significant differences between the graphene domain shapes on different regions (grains) of the Cu substrate.

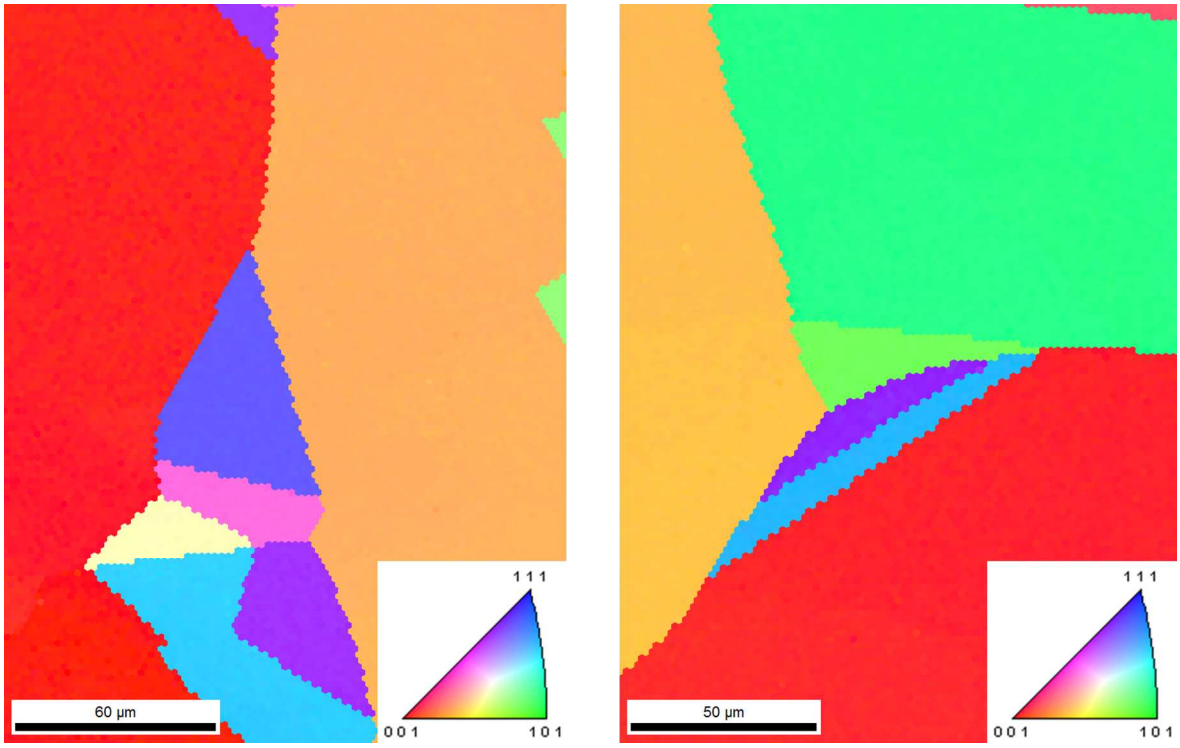

Figure S2| EBSD maps of Cu surface, with colours corresponding to the Cu crystal plane normals indexed with the colour key (inset) (corresponding to regions shown in **Figure S1**).

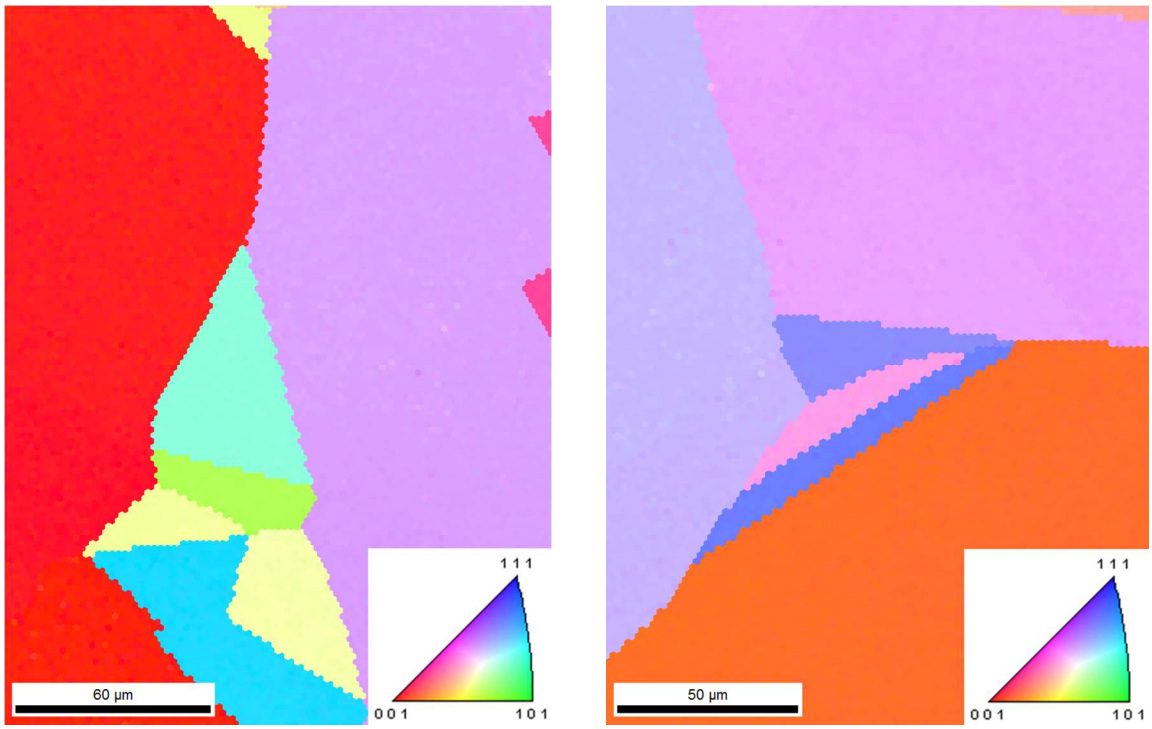

Figure S3| EBSD maps of the in-plane rotation of Cu grains, with colours corresponding to the Cu crystal plane perpendicular to the horizontal axis of the map indexed with the colour key (inset).

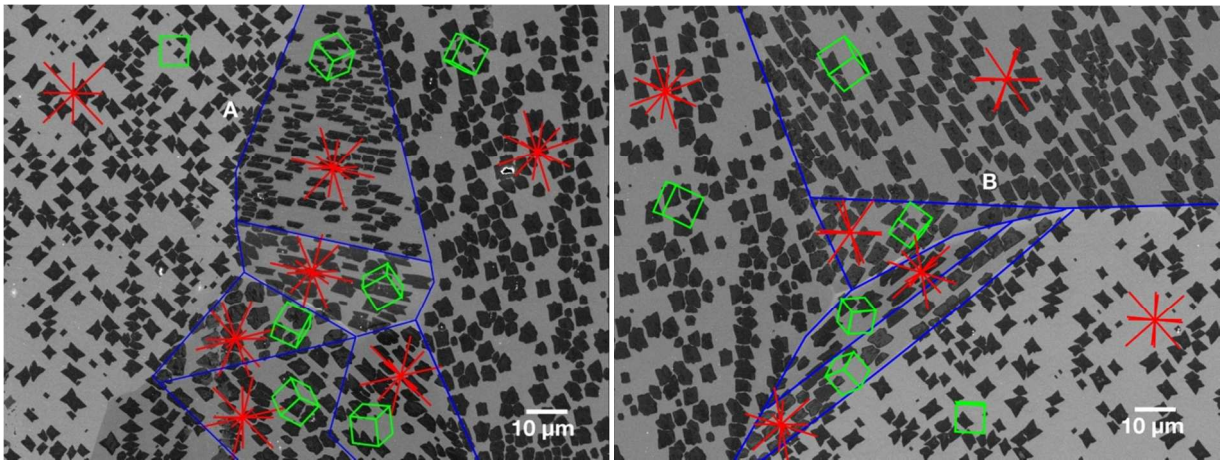

Figure S4| Normal incidence SEM images comparing the orientation of LPCVD graphene domains with the orientation of the Cu substrate derived from the EBSD mapping, with: crystal orientations as green cubes; projections of the {110} directions as red 'jacks' with longer arm lengths indicating closer to inplane directions; and grain boundaries as blue lines. A and B indicate regions displayed in **Fig. S5.**

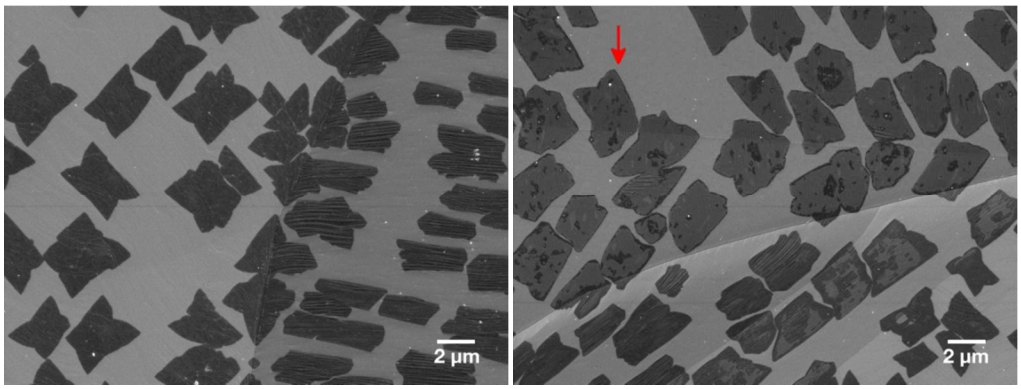

Figure S5| SEM images showing the change of shape and orientation of LPCVD graphene domains at Cu grain boundaries. Left image shows region A from **Figure S4**, with domains growing over Cu{001} (left side) and Cu{769} (right side) and consequently changing from 4 lobed parallel-sided domains to hexagonal-edged elongated domains. Right image shows region B from **Figure S5**. This region is also represented in Figure 1c of main text, with the red arrow indicating domains spanning across two misorientated grains that share the Cu(101) surface normal. Domains orientate to [-101] direction of each underlying grain.

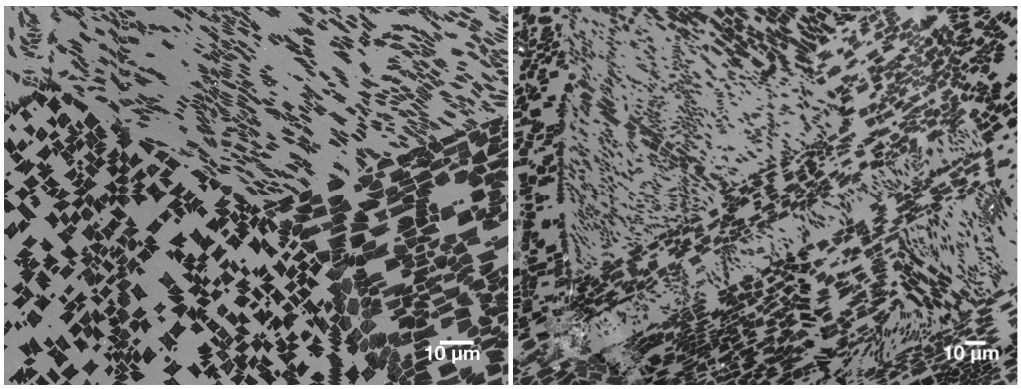

Figure S6| SEM images demonstrating significant change in LPCVD graphene domain shape and orientation over different Cu grains. Left image shows three predominant Cu grains, and consequently three representative shapes of graphene domains with specific orientations. Right image shows a complex Cu surface with many grain boundaries. Nonetheless, graphene domains consistently change shape and orientation on different Cu grains.

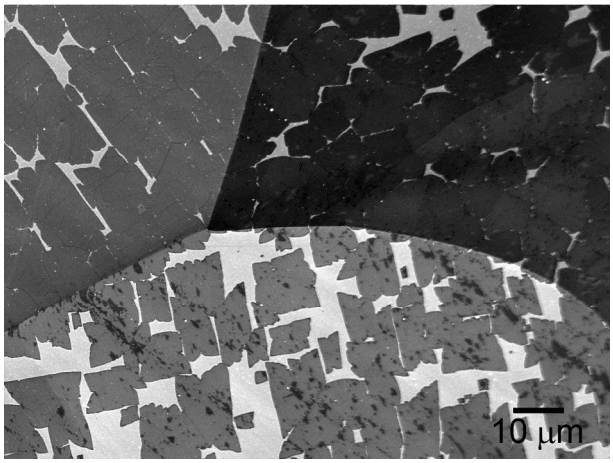

Figure S7| SEM image of larger LPCVD graphene domains. Growth time was extended to 10 minutes and stopped just before full-scale coverage was achieved. Further extending the growth time yields uniform full-scale coverage. The normal orientation of Cu grains can be inferred due to the shape and orientation of graphene domains *e.g.* bottom grain: Cu{001}, upper left grain: near Cu{111}. Domains on Cu{101} have frequently coalesced along parralel sided and oriented edges.

AFM topography image of Cu surface morphology

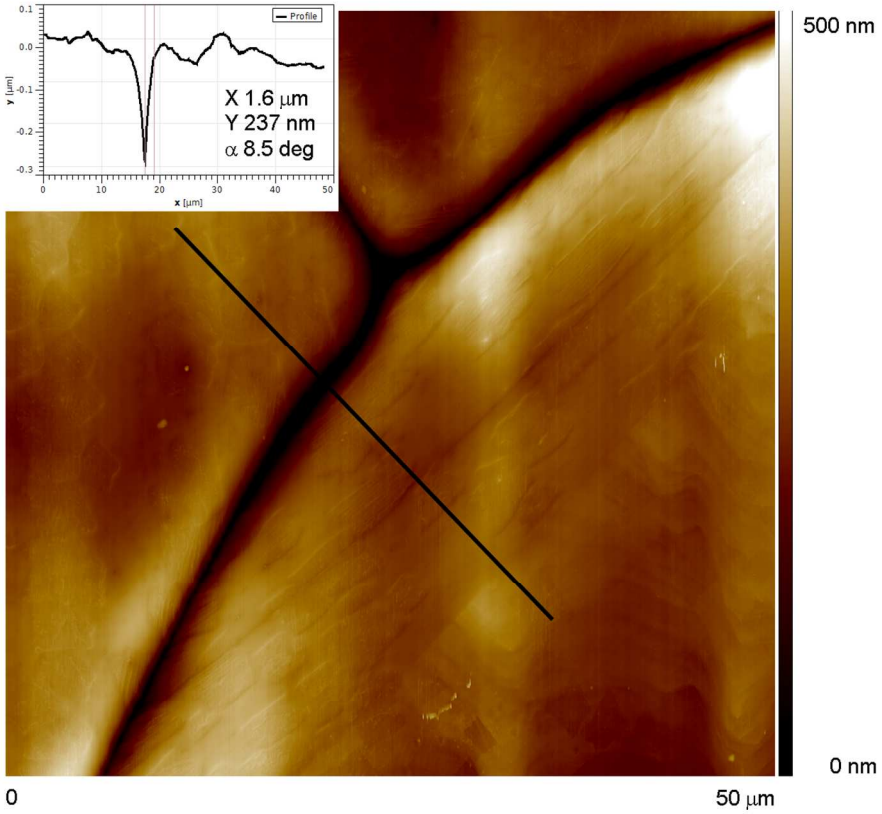

Figure S8| AFM topography image recorded on the region presented in Figure 1 and Figure 4. Topographical variations can be seen across the Cu surface, with the Cu evaporation rate varying on different Cu grains and on regions covered by graphene domains. A maximum height difference of 200 nm is measured via line profile across the grain boundary. No correlation is observed between the surface morphology presented in Figure S8 and the two-dimensional Raman map presented in Figure 5, indicative that Raman thickness measurements are reliable and an effect of height differences across the Cu substrate can be neglected.

Edge angle orientation of individual LPCVD graphene domains on different Cu orientations

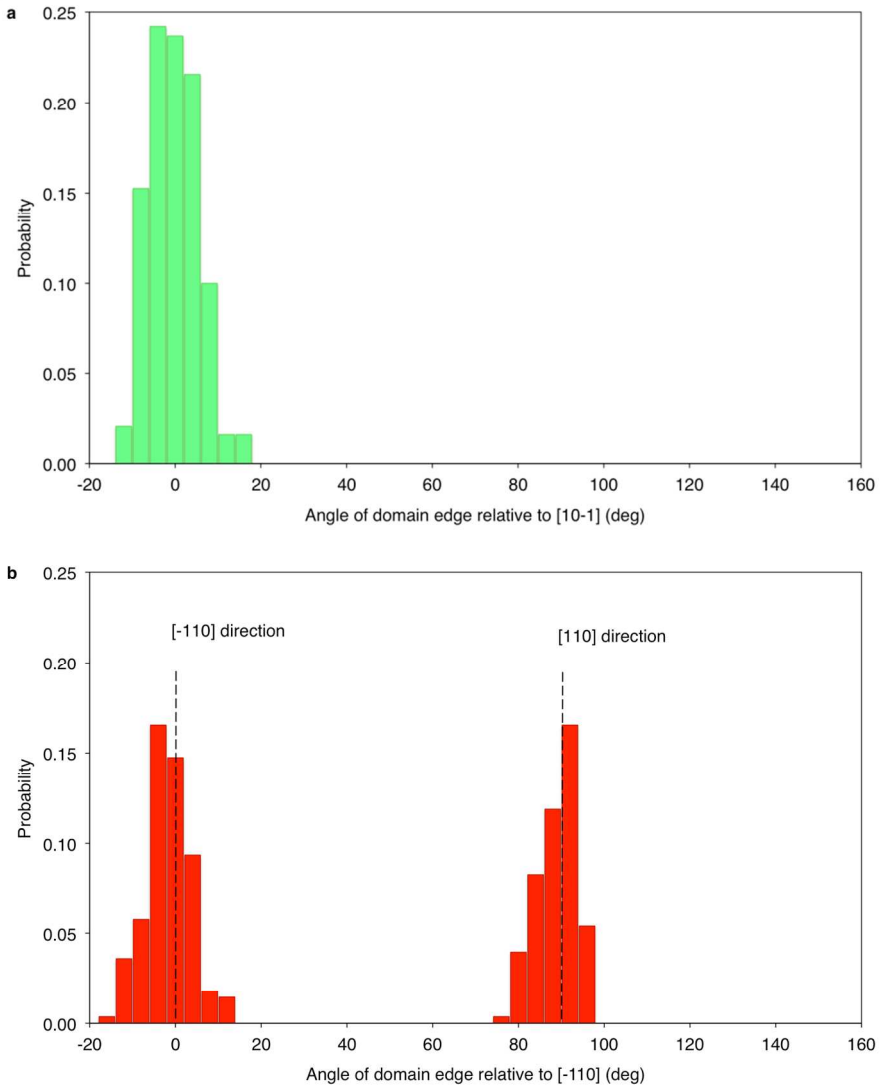

Figure S9| Distribution of the edge angle of graphene domains on Cu surfaces. **a**, The edge orientation was measured for over 150 graphene domains grown on Cu(101) (determined by EBSD). The resulting distribution is centred 2˚ from the [-101] direction (standard deviation of 6˚). **b**, The edge orientation was measured for over 300 domains on Cu(001) (determined by EBSD). The resulting distribution is bimodal with 53 % of the measurements distributed around the [-110] direction and 47 % distributed around the [110] direction. The two modes are -4˚ misaligned (standard deviation 5˚) and 3˚ misaligned (standard deviation 4˚), respectively.

Influence of crystallographic orientation on LPCVD graphene domain size and growth rate

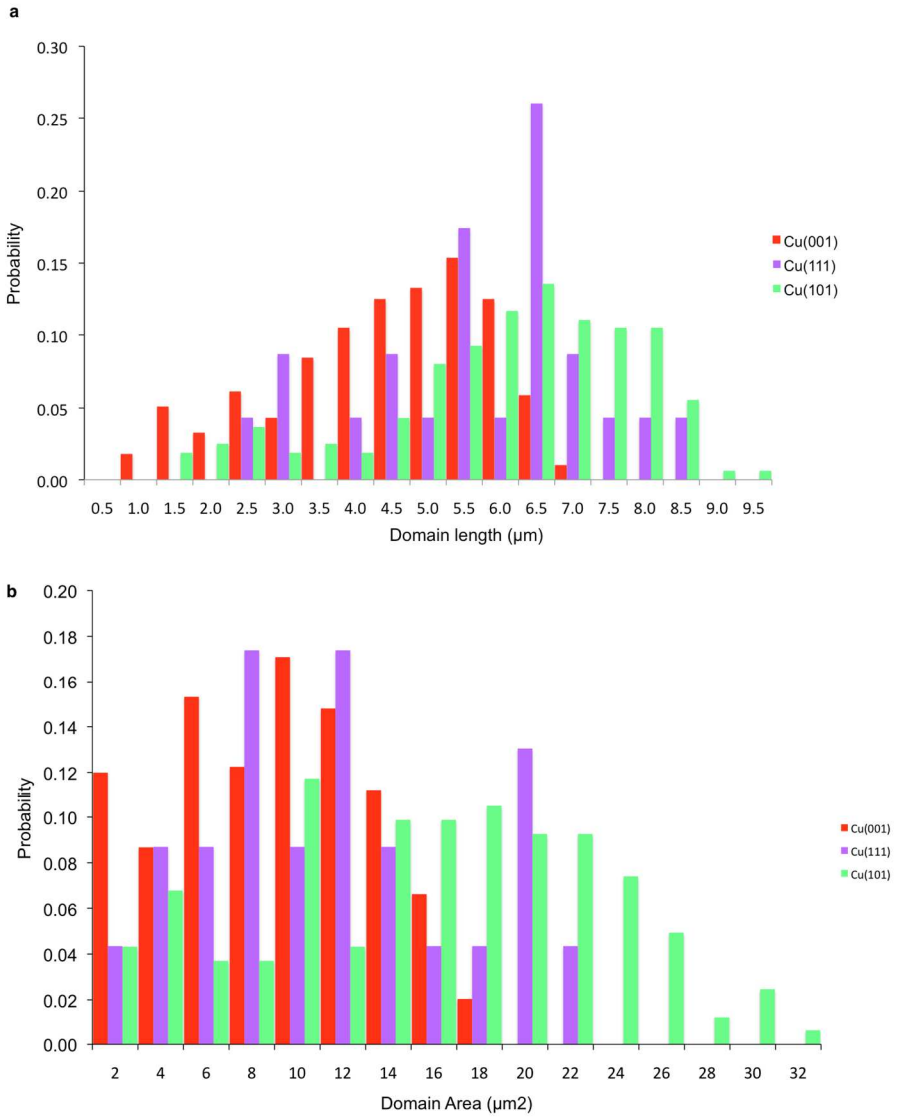

Figure S10| Influence of Cu crystallographic orientation on LPCVD graphene domain size, determined using Image J analysis. **a,** Distritution of maximum feret diameters of domains on different Cu crystallographic orientations. **b,** Distribution of feret area of domains on different Cu crystallographic orientations. Domain length, domain area, and hence domain growth rate, are dependant on the Cu crystallographic orientation, such that Cu{101} > Cu{111} > Cu{001}.

Stepped surfaces

Cu(335) and Cu(535) are ~13˚ tilted from Cu(111). Consequently, both are stepped surfaces[4], exhibiting terraces with (111) atomic packing and lattice steps running parallel to [1-10]. Graphene domains on Cu(335) and Cu(535) are elongated parallel to [1-10]. This indicates that preferential growth occurs to some degree along the terraces rather than over steps. However, the edges of these domains are hexagonally shaped and align to the components of [10-1] and [0-11] within the (111) terraces on the stepped surface, namely [50-3] and [0-53]. Therefore it appears that although terrace and lattice steps may promote elongated domains, a preference still exists for edges to orient parallel to the <110> direction.

Cu(769), tilted ~9˚ from (111), was also investigated (triangle-shaped purple grain at centre of Figure S2 and Figure S4). This domain is significantly larger than Cu(335)/Cu(535) so the influence of grain boundaries will be reduced. Domains on Cu(769) showed similar behaviour to Cu(335)/Cu(535) with the elongated edge aligning to [1-10] and hexagonal edges to the component of <110> within the surface plane.

Owing to the absence of parallel edges, the six-lobe star-shaped domains on Cu(103) display only minor edge alignment with [-311]. Cu(103) is again a stepped surface, but in this case terraces have (001) atomic packing and lattice steps run parallel to [010]. Consequently, a number of competing factors may influence domain growth on Cu(103): the preference for edge orientations parallel with [110] and [1-10] directions on the (001) terraces (corresponding to [-331] and [-3-31] in the surface plane); preferential growth in the [010] direction parallel to steps; and growth dictated by the six-fold symmetrical graphene lattice. The observation of 6-lobe domains with minimal edge alignment illustrates that growth is dictated by a combination of these factors, indicating that Cu(103) provides less control of domain growth compared to other orientations.

Alignment of APCVD hexagonal graphene domains

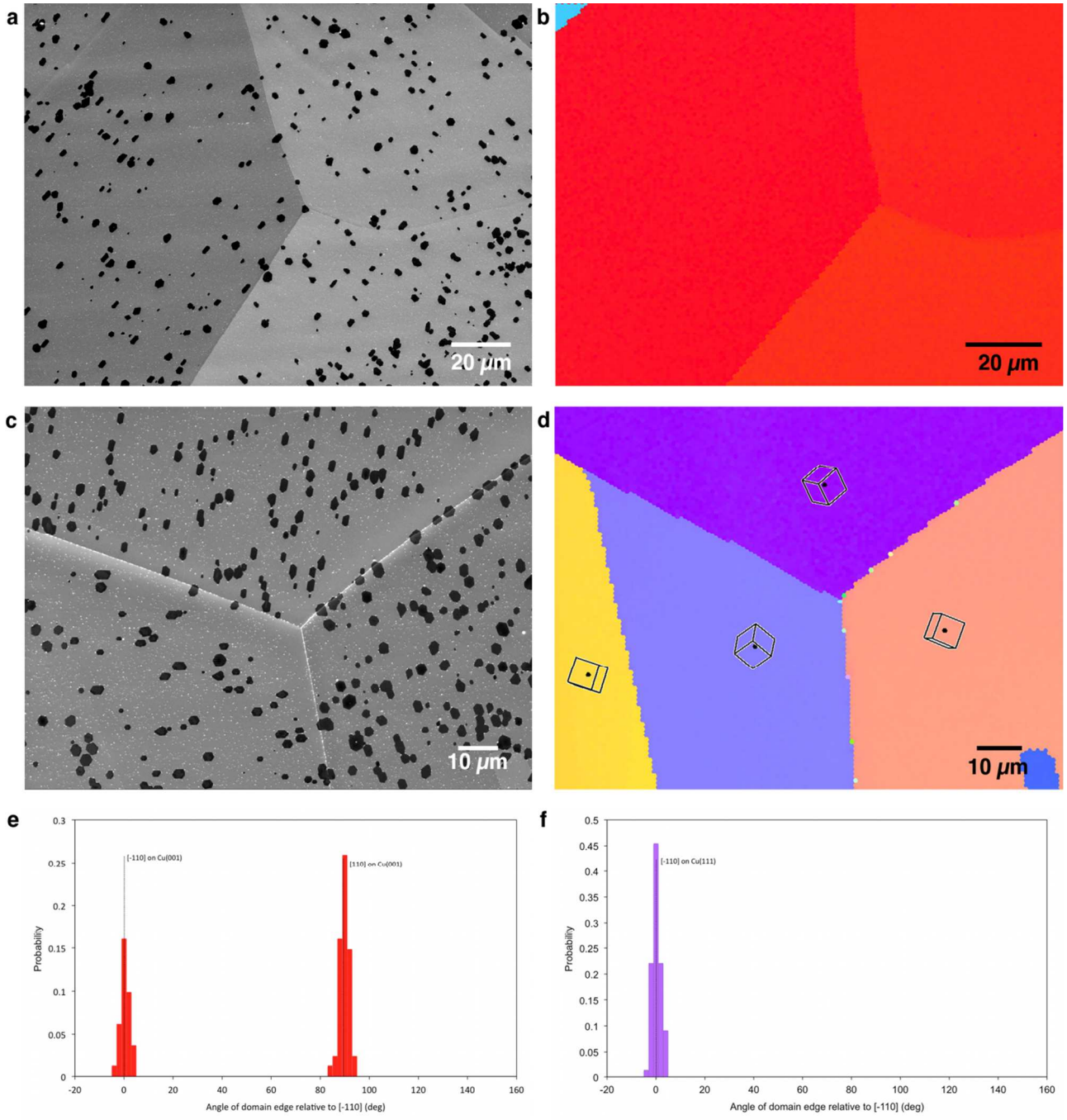

Figure S11| Edge alignment of hexagonal APCVD graphene domains grown on high purity (99.999 %) *Alfa Aesar* Cu foil. **a, c,** SEM images demonstrating variation in edge alignment of hexagonal graphene domains on different Cu grains. **b**, **d**, Associated EBSD maps with colours corresponding to the Cu crystal plane normals indexed and unit cubes demonstrating crystallographic orientations. Comparing the SEM and EBSD images it is apparent that hexagonal domains orientate to two 90˚ rotated <101> directions on grains close to Cu{001} (e.g. red) and to a single <101> direction on grains close to Cu{111} (e.g. purple and blue grains). Less alignment is observed on grains misoriented between Cu{001} and Cu{101} (e.g. orange and yellow). **e,** Distribution of the edge angle of hexagonal APCVD graphene domains grown on high purity (99.999 %) *Alfa Aesar* Cu foil with grain orientations near Cu{001}, measured for over 50 graphene domains. **f,** Distribution of the edge angle of hexagonal APCVD graphene domains grown on high purity (99.999 %) *Alfa Aesar* Cu foil with grain orientations near Cu{111}, measured for over 50 graphene domains.

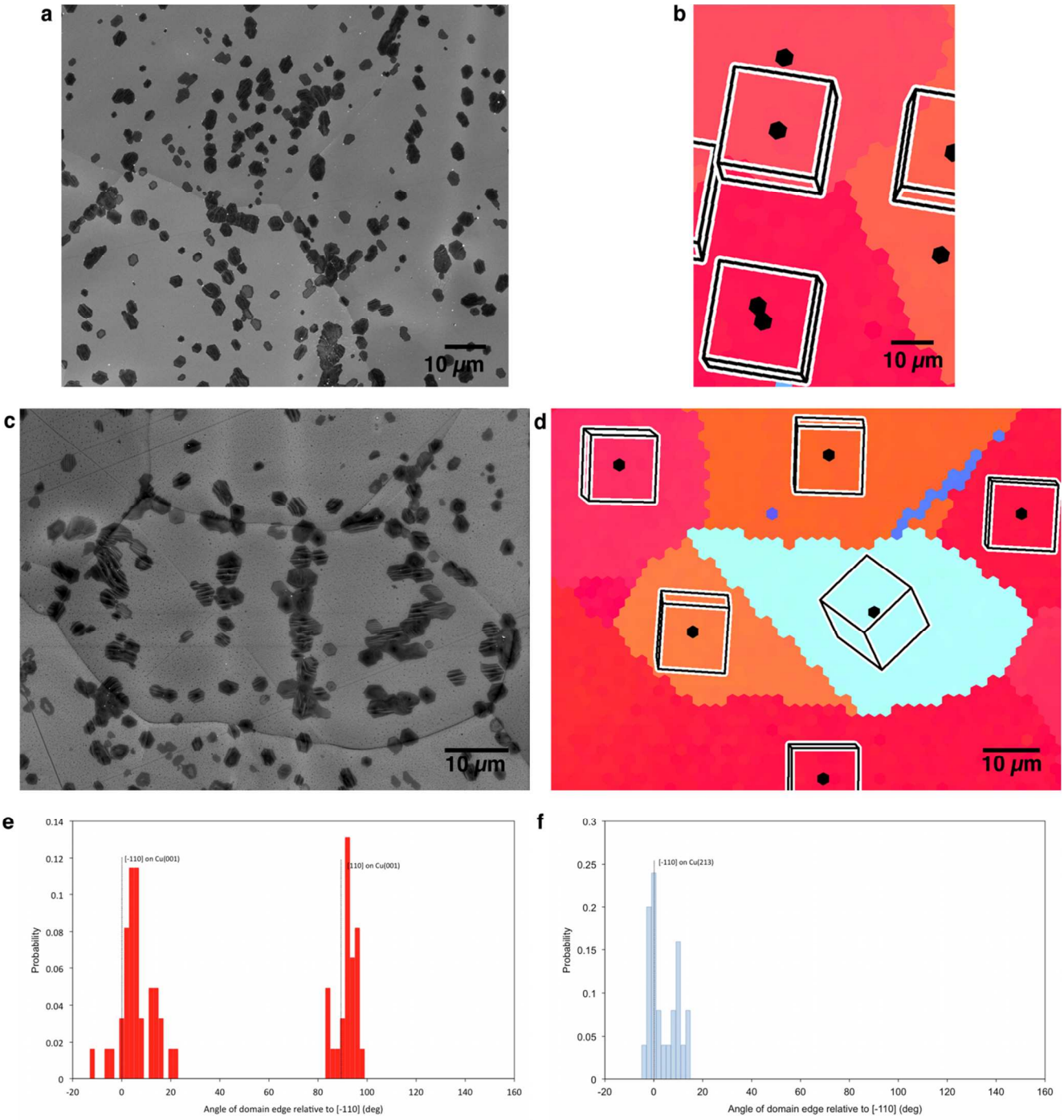

Figure S12| Edge alignment of hexagonal APCVD graphene domains grown on low purity (99.8 %) *Alfa Aesar* Cu foil. **a, c** SEM images demonstrating variation in edge alignment of hexagonal graphene domains on different Cu grains. **b, d,** Associated EBSD map with colours corresponding ot the Cu crystal plane normal indexed and unit cubes demonstrating crystallographic orientations. Comparing the SEM and EBSD images it is apparent that hexagonal domains orientate to two 90˚ rotated <101> directions on grains close to Cu{001} (e.g. red) and to a single <101> direction on grains close to Cu{111} (e.g. light blue Cu(213). **e,** Distribution of the edge angle of hexagonal APCVD graphene domains grown on low purity (99.8 %) *Alfa Aesar* Cu foil with grain orientations near Cu{001}, measured for over 60 graphene domains. **f,** Distribution of the edge angle of hexagonal APCVD graphene domains grown on low purity (99.8 %) *Alfa Aesar* Cu foil with grain orientations near Cu{111}, measured for over 30 graphene domains.

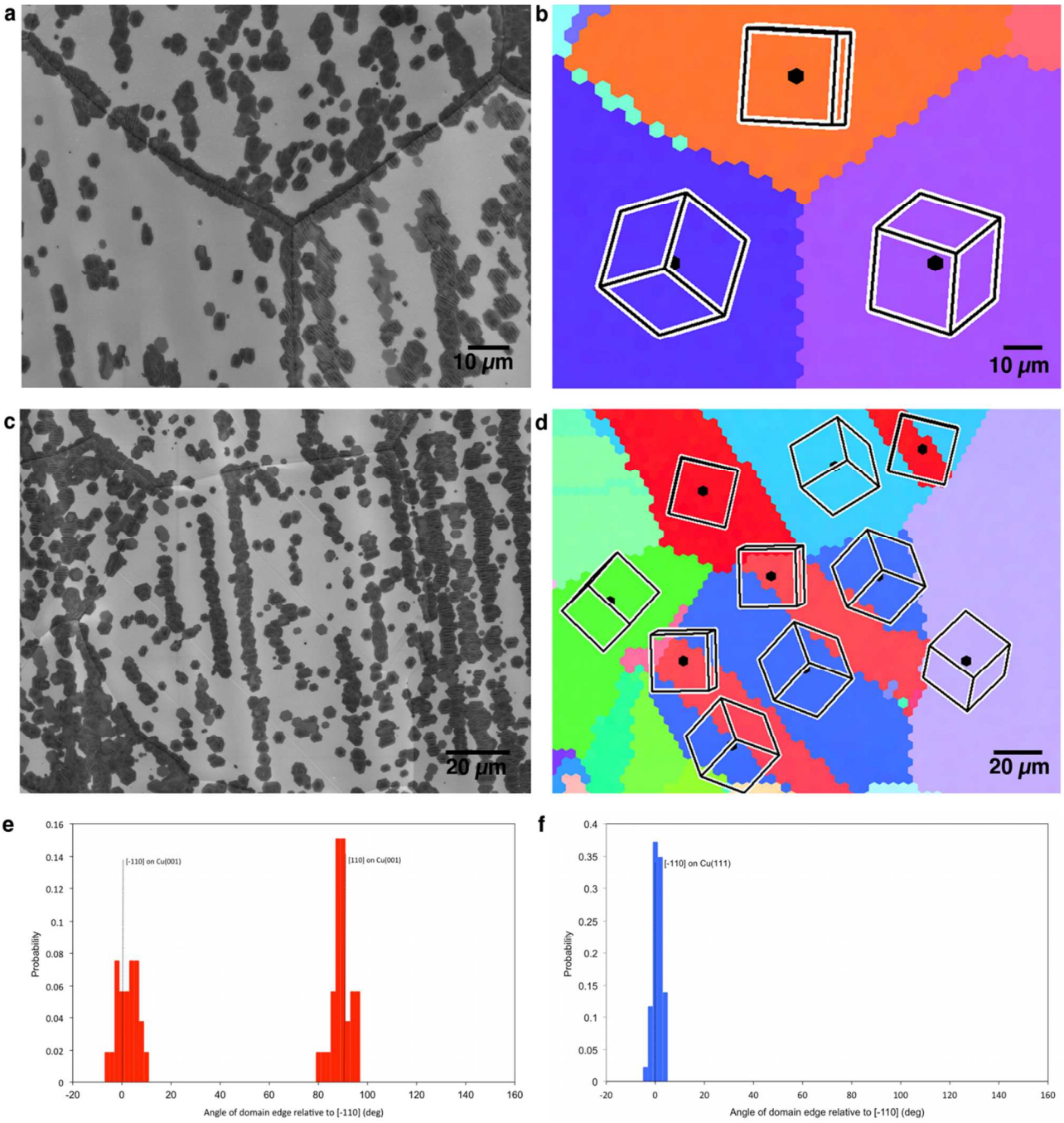

Figure S12| Edge alignment of hexagonal APCVD graphene domains grown on low purity (99.9%) *Goodfellow* Cu foil. **a, c,** SEM images demonstrating variation in edge alignment of hexagonal graphene domains on different Cu grains. **b**, **d,** Associated EBSD maps with colours corresponding to the Cu crystal plane normals indexed and unit cubes demonstrating crystallographic orientations. Comparing the SEM and EBSD images it is apparent that hexagonal domains show significant alignment to <101> direction on grains close to Cu{111} (e.g. purple and blue grains) and Cu{101} (e.g. green). Domains align to two 90˚ rotated <101> directions on grains close to Cu{101} (e.g. red, pink, orange). **e,** Distribution of the edge angle of hexagonal APCVD graphene domains grown on low purity (99.9 %) *Goodfellow* Cu foil with grain orientations near Cu(001), measured for over 50 graphene domains. **f,** Distribution of the edge angle of hexagonal APCVD graphene domains grown on low purity (99.9%) *Goodfellow* Cu foil with grain orientations near Cu(111), measured for over 50 graphene domains.

Raman spectroscopy

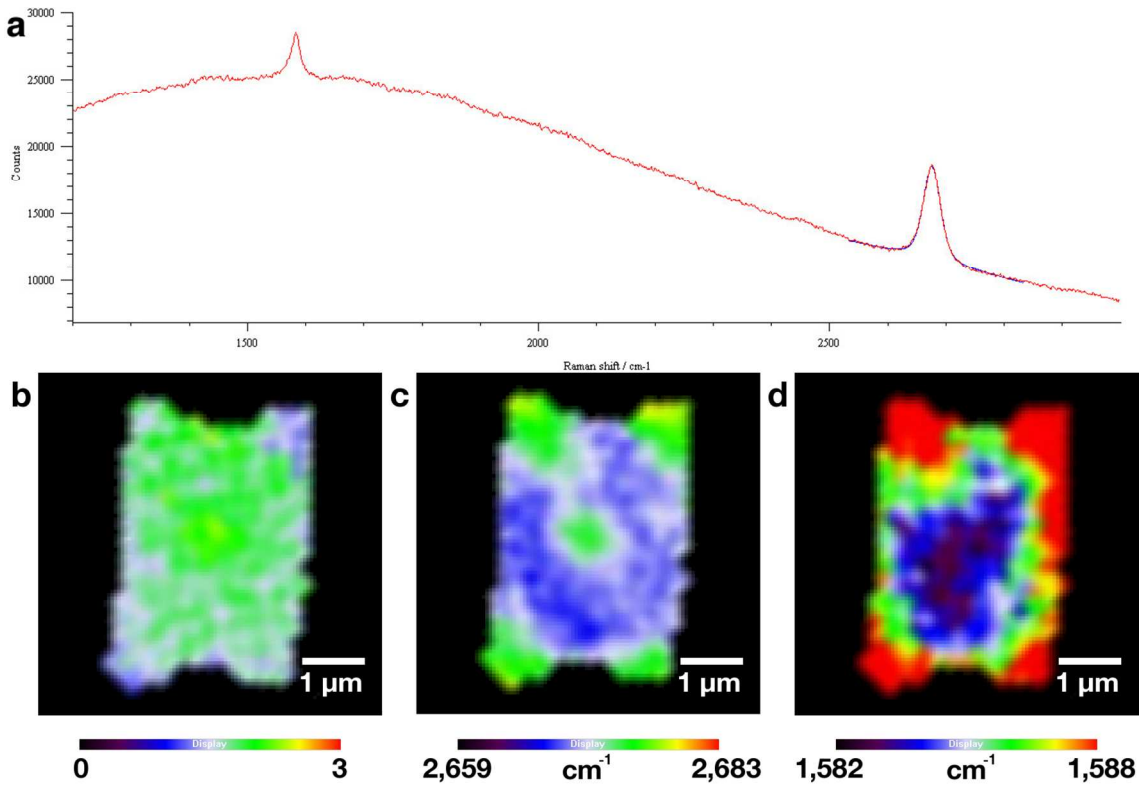

Figure S13| a, Representative raw Raman spectrum from Figure 5, **b, c, d,** High resolution spatially resolved Raman spectroscopy of an individual graphene domain from Cu{001} representing I_{2D}/I_G, 2D position and G position respectively.

Raman spectroscopy provides a non-destructive analysis of the number of layers and quality of the graphene domains, with the G peak (~1580 cm^{-1}), 2D peak (~2685 cm^{-1}) and D peak (~1350 cm^{-1}) being key features of the graphene spectrum (see Figure S12a)[2]. The intensity ratio between the 2D and G peaks, I_{2D}/I_G, indicates the number of layers present in CVD graphene[3]; if $I_{2D}/I_G>2$ then a sample can be regarded as single layer graphene, if $1<I_{2D}/I_G<2$ then bilayer graphene is present, and if $I_{2D}/I_G<1$ then 3 or more layers are present. The intensity of the D peak indicates defects in the graphene[2].

While we attempted to map the intensity of the D peak across the 90 x 90 µm region depicted in Figure 5, and across a single graphene domain in Figure S13 with high resolution scanning, the D peak was invariably absent. This indicates that the graphene domains are of the highest quality with minimal defects. The absence of the D peak also suggests that the domains are single crystals, as grain

boundaries between misorientated domains within a polycrystalline domain produce a detectable D peak[4].

The positions of the 2D and G peaks can indicate the presence of substrate-induced electrical doping[5-7] and strain in graphene domains. The G peak up-shifts for both electron and hole doping, while the 2D peak down-shifts for electron doping and up-shifts for hole doping[2, 8, 9]. In comparison, the 2D and G peaks down-shift for tensile strain[10, 11] and up-shift for compressive strain[12]. Both substrate-induced doping and strain may be present in graphene domains on Cu foil, with influences dependent on the crystallographic orientation. Figure 5b and Figure 5c present maps of the 2D and G peak position respectively, and should be viewed collectively and compared to Figure 1d when drawing conclusions. Traversing the figures from the bottom-right to the top-left, the 2D peak position systematically down-shifts across different crystallographic orientations ranging from ~2675 - 2680 cm^{-1} on Cu{001}, ~2670 - 2675 cm^{-1} on Cu{535} and ~2660 - 2665 cm^{-1} for Cu{103}. Meanwhile, in Figure 4c the G peak position is observed to be somewhat higher on Cu{001}, between ~1595 - 1600 cm^{-1}. Intercalation of oxygen between domains and the substrate preferentially on Cu{001} may cause this anomaly[13]. Otherwise, a minor down-shift in G peak position is observed from the Cu{535} orientation at ~1588 cm^{-1} and the Cu{335}, Cu{103} and Cu{101} orientations at ~1580 - 1585 cm^{-1}. Tensile strain can explain the variations observed in the 2D and G peak position across different crystallographic orientations. Strain could be introduced into the graphene domains as Cu steps and hillocks accumulate underneath them during growth[14]. More generally, strain may originate because of the lattice mismatch between the graphene network and the Cu surface. Such influences will be dependent on the atomic spacing of the Cu surface and therefore crystallographic orientation as indicated by computational modelling.

To verify that tensile strain originates from interactions with the Cu substrate, graphene domains were transferred onto SiO_2/Si and Raman spectra were again recorded. The G and 2D peak were

located at 1594 cm^{-1} and 2685 cm^{-1} respectively for transferred domains. This confirms that the peak positions down-shift due to interactions with the Cu substrate. The 2D position downshifts by a maximum of ~25 cm^{-1} across the different crystallographic orientations, corresponding to a maximum possible tensile strain of 0.18 %[11]. However, the influence of substrate-induced doping, which may even vary between different Cu orientations, could also be contributing to the observed shift in Raman peak positions and cannot be entirely excluded.

A more detailed examination of a single graphene domain on Cu{001} is presented in Figure S13. The intensity ratio (Figure S13b) is unchanging across the domain indicating uniform bilayer graphene. The 2D and G peak positions (Figure S13c and S13d) increase at the tips of the four lobes of the domain, regions that correspond to the growth front of the graphene domain. An increase in the 2D peak position is also observed at the centre of the domain at the nucleation site. The shift in peak positions may originate from (i) increased oxygen intercalation, (ii) variations in the interaction between the domain and the substrate, or (iii) variations in the localised strain of the graphene domain at these regions.

Computational modeling

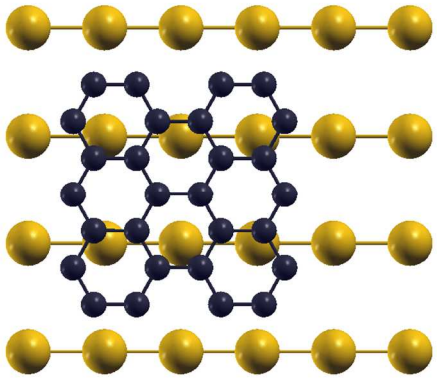

Figure S14| Graphene cluster C_{28} on Cu(101) oriented with armchair edge parallel to [-101] demonstrating lattice mismatch when compared to Figure 3g.

Taking into account the graphene and Cu(101) surface structural characteristics, we deposited a representative graphene cluster, C_{28}, with its zigzag edge ($a_{cc}\sqrt{3}$ = 2.46 Å) aligned along to the [-110] direction ($a\sqrt{2}/2$ = 2.556 Å) and the armchair edge ($3a_{cc}$ = 4.26 Å) parallel to the [001] direction (unit cell = 3.615 Å) (Figure 3g). Alternative orientations of C_{28} on the Cu(101) surface produces a conspicuous lattice mismatch (Figure S14).

Supporting Information references

1. Van Hove, M. A.; Somorjai, G. A. *Surf. Sci.* **1980,** 92, 489-518.
2. Ferrari, A. C. *Solid State Commun.* **2007,** 143, 47-57.
3. Reina, A.; Jia, X.; Ho, J.; Nezich, D.; Son, H.; Bulovic, V.; Dresselhaus, M. S.; Kong, J. *Nano Lett.* **2009,** 9, 30-35.
4. Yu, Q.; Jauregui, L. A.; Wu, W.; Colby, R.; Tian, J.; Su, Z.; Cao, H.; Liu, Z.; Pandey, D.; Wei, D.; *et al. Nat. Mater.* **2011,** 10, 443-449.
5. Giovannetti, G.; Khomyakov, P. A.; Brocks, G.; Karpan, V. M.; van den Brink, J.; Kelly, P. J. *Phys. Rev. Lett.* **2008,** 101, 026803.
6. Ren, Y.; Chen, S.; Cai, W.; Zhu, Y.; Zhu, C.; Ruoff, R. S. *Appl. Phys. Lett.* **2010,** 97, 053107.
7. Varykhalov, A.; Scholz, M. R.; Kim, T. K.; Rader, O. *Phys. Rev. B* **2010,** 82, 121101.
8. Wang, W. X.; Liang, S. H.; Yu, T.; Li, D. H.; Li, Y. B.; Han, X. F. *J. Appl.Phys.* **2011,** 109, 07C501.
9. Das, A.; Pisana, S.; Chakraborty, B.; Piscanec, S.; Saha, S. K.; Waghmare, U. V.; Novoselov, K. S.; Krishnamurthy, H. R.; Geim, A. K.; Ferrari, A. C.; *et al. Nat. Nanotechnol.* **2008,** 3, 210.
10. Mohiuddin, T. M. G.; Lombardo, A.; Nair, R. R.; Bonetti, A.; Savini, G.; Jalil, R.; Bonini, N.; Basko, D. M.; Galiotis, C.; Marzari, N.; *et al. Phys. Rev. B* **2009,** 79, 205433.
11. Zabel, J.; Nair, R. R.; Ott, A.; Georgiou, T.; Geim, A. K.; Novoselov, K. S.; Casiraghi, C. *Nano Lett.* **2012,** 12, 617-621.
12. Frank, O.; Tsoukleri, G.; Parthenios, J.; Papagelis, K.; Riaz, I.; Jalil, R.; Novoselov, K. S.; Galiotis, C. *ACS Nano* **2010,** 4, 3131-3138.
13. Walter, A. L.; Nie, S.; Bostwick, A.; Kim, K. S.; Moreschini, L.; Chang, Y. J.; Innocenti, D.; Horn, K.; McCarty, K. F.; Rotenberg, E. *Phys. Rev. B* **2011,** 84, 195443.